The effect of terminal sterilization on structural and biophysical properties of a decellularized collagen-based scaffold; implications for stem cell adhesion

Andrea M. Matuska and **Peter S. McFetridge**

J. Crayton Pruitt Family, Department of Biomedical Engineering, University of Florida, Florida

Abstract

Terminal sterilization induces physical and chemical changes in the extracellular matrix (ECM) of *ex vivo*-derived biomaterials due to their aggressive mechanism of action. Prior studies have focused on how sterilization affects the mechanical integrity of tissue-based biomaterials but have rarely characterized effects on early cellular interaction, which is indicative of the biological response. Using a model fibro-cartilage disc scaffold, these investigations compare the effect of three common sterilization methods [peracetic acid (PAA), gamma irradiation (GI), and ethylene oxide (EtO)] on a range of material properties and characterized early cellular interactions. GI and EtO produced unfavorable structural damage that contributed to inferior cell adhesion. Conversely, exposure to PAA resulted in limited structural alterations while inducing chemical modifications that favored cell attachment. Results suggest that the sterilization approach can be selected to modulate biomaterial properties to favor cellular adhesion and has relevance in tissue engineering and regenerative medicine applications. Furthermore, the study of cellular interactions with modified biomaterials *in vitro* provides information of how materials may react in subsequent clinical applications.

Keywords

cell adhesion; sterilization; surface modification; tissue engineering; collagen

INTRODUCTION

Tissue grafting has been used clinically for more than 100 years to successfully regenerate nerve, skin, bone, and other tissues of the musculoskeletal system.[1–4] Pretreatment of *ex vivo*-derived biomaterials for regenerative medicine or tissue engineering applications vary widely.[5,6] Introduction of procedures, such as decellularization, to remove cellular antigens and reduce immunogenicity have the potential to eliminate the need for autologous or patient matched grafts for direct clinical use.[7,8] Additionally, terminal sterilization is a critical step used to eliminate bacteria and viruses.[7,9] Compared to synthetic or metal implant materials, sterilization of biological tissues can be problematic as these processes

Correspondence to: P. S. McFetridge (pmcfetridge@bme.ufl.edu).

typically have an aggressive mechanism of action that can adversely affect natural tissue properties. Alteration of natural material properties such as biomechanics, physical structure, and surface chemistry potentially mitigate the benefits of using naturally derived materials for tissue regeneration by modifying intrinsic factors that direct cell adhesion and guide tissue regeneration.[10–13]

Gamma irradiation (GI), ethylene oxide (EtO), and peracetic acid (PAA) are commonly used tissue graft sterilization methods and chosen for comparison because they sterilize via fundamentally different mechanisms.[14–17] Some sterilization studies with synthetic materials have used disinfection with ethanol 70% as a control, but this treatment is not used clinically due to its ineffectiveness in removing bacterial spores and viruses.[18] Moreover, treatment with 70% ethanol induces protein denaturation and tissue dehydration that influences scaffold structure significantly altering cellular interactions.[19,20] Another well-known sterilant, glutaraldehyde, was not assessed in these investigations due to the excessive crosslinking that typically results in graft encapsulation, poor cell infiltration, and in the case of numerous vascular applications long term failure from calcification.[7,21]

GI has been shown to destroy nucleic acids through two mechanisms; either directly by ionizing radiation or indirectly by hydroxyl radicals generated through radiolysis in the presence of water.[14] While GI has not been associated with chemical changes of soft tissue, it has been shown to produce structural and mechanical changes that may effect cellular interactions.[22,23] The effects of radiation on collagen fibers include either direct scission of alpha polypeptide chains or crosslinking in the presence of free radicals.[14,15,24,25]

EtO is a diffusive gas and a strong alkylating agent that denatures DNA and proteins by addition of alkyl groups thereby interfering with normal cellular processes. As a byproduct of these reactions EtO produces the toxic derivatives ethylene chlorohydrin and ethylene glycol.[16] Critical with this approach is ensuring sufficient diffusion into tissues and successive diffusion of remnant EtO and its derivatives out.[4]

Lastly, PAA is a strong oxidizing agent that through the transfer of electrons oxidizes numerous chemical groups including those on cell membranes thus initiating cell death.[26,27] PAA has been shown to inactivate viruses, fungi, and bacteria at low concentrations.[28] It also generates low toxicity byproducts such as water, oxygen, and carbon dioxide.[17]

In this study, decellularized porcine temporomandibular joint (TMJ) discs were used as an *ex vivo* derived fibrocartilage tissue scaffold. Previous studies have determined that decellularization of the TMJ disc with sodium dodecyl sulfate (SDS) limits biomechanical and physical changes to the ECM compared to other methods including ethanol/acetone and Triton-X.[6] The TMJ disc is an articulating fibrocartilage disc composed predominantly of Type I collagen that cushions and allows proper movement between the mandible and temporal bone of the TMJ. The TMJ disc offers a unique perspective given its similarities to both hyaline cartilage and tendon.[29]

Various studies have assessed how sterilization affects biomechanical properties of tissue grafts, but rarely how these changes influence initial cell attachment, a prerequisite for tissue regeneration and remodeling.[15,23,30] Cell adhesion is also important in tissue engineering

applications where initial cell concentrations may be limited. Therefore, the purpose of this study was to evaluate extracellular matrix variations resulting from different terminal sterilization strategies and to correlate these findings, including biomechanics, ultrastructure, and surface chemistry, with initial cell interaction. By further understanding how tissue properties are altered by sterilization techniques, methods can be devised to modify ECM-based biomaterials to encourage tissue regeneration, namely by facilitation of cell adhesion.

MATERIALS AND METHODS

Tissue collection and processing

Porcine TMJ discs were obtained from animals aged 6–9 months (IACUC # 201207534, Animal Technologies, Tyler, TX) and dissected as previously described.[6] From the intermediate region of the disc, 2–3 six mm diameter punches were removed using a disposable biopsy punch (Miltex, York, PA). Full-sized discs and punches were decellularized for 24 h in a 1% SDS solution under agitation (100 rpm) with one change of SDS solution at 12 h. Discs were agitated in successive PBS solutions (pH 7.4) to remove SDS, and then treated with 150 U/mL DNase (Sigma-Aldrich, St. Louis, MO) at 37°C for 16 h to fragment and facilitate the removal of residual DNA.

Decellularized tissue scaffolds were split into three different groups for sterilization. Tissue in group one was sterilized in 0.2% PAA/4% ethanol solution under agitation for 6 h and rinsed in sterile PBS until pH was balanced at 7.4. Tissue was aseptically frozen and lyophilized (Millrock Technology, Kingston, NJ) and stored until use. Tissue in groups two and three were lyophilized and either gamma irradiated or EtO sterilized. GI was performed in a J.L. Sheperd Mark I cesium-137 irradiator for 15 h with a dose of ~13 kGy. EtO sterilization used a dedicated tabletop Anprolene AN74J sterilizer (Anderson Products, Health Science Park, NC) with an EtO dose of 700 ppm over a 12 h cycle with at least an additional 2 h purge/aeration step. Sterilization was ensured with a dosimeter and biological indicator. Discs were then ventilated for two additional weeks to allow residual EtO and byproduct clearance. Decellularized and freeze dried tissue, which was not sterilized served as controls where necessary. A summary of the tissue processing is shown in Figure 1.

Biomechanical evaluation

Six millimeter diameter discs ($n = 6$) were hydrated at room temperature in PBS for 24 h and equilibrated at 37°C for 5 min before testing. Discs were placed in a hydrated testing chamber in a Biomomentum Mach-1 micromechanical system (Biomomentum, Laval, Quebec, Canada) and subject to cyclic compression tests consisting of 15 cycles at 10% and 20% strain to simulate normal-physiologic and extreme-physiologic strain values, respectively.[31] Strain was defined as $\varepsilon = \Delta L/L_0$ with ΔL being the change in sample thickness and L_0 being the original samples thickness. Stress was defined as $\sigma = F/A$ with F being compressive force and A being the cross-sectional area of the disc. Compressive moduli were defined as $E = \sigma/\varepsilon$, where instantaneous compressive modulus (E_{inst}) was calculated using peak stress for the first cycle, while steady state compressive (E_{ss}) modulus was determined using peak stress for the last cycle.[32]

Surface chemistry

Raman and Fourier transform infrared (FTIR) spectroscopy were performed to evaluate differences in surface chemistry as a result of sterilization method. Both methods were chosen for completeness, since certain stretching modalities weakly observed by Raman scattering are more strongly observed by FTIR absorption.[33] FTIR was acquired using a Thermo Electron Nicolet Magna 760 FTIR (West Palm Beach, FL) and Raman via a Renishaw inVia Raman microscope (Gloucestershire, UK). FTIR spectra were obtained from wavenumbers 600–4000 cm^{-1} with spectral resolution of 1.93 cm^{-1}. Raman spectra were collected from Raman shift range 200–1700 cm^{-1} with spectral resolution of 0.82 cm^{-1}. Multiple spectra were obtained from different locations and surfaces of the discs ($n = 9$). Using Biorad Informatics software (Philadelphia, PA) background was removed from spectra, height normalized then averaged.

Evaluation of surface microarchitecture

Scanning electron microscopy (SEM) was performed to evaluate the surface structure of sterilized and control discs. Briefly, samples were fixed in 2.5% glutaraldehyde (Sigma-Aldrich, St. Louis, MO) and treated with 1% osmium tetroxide. They were washed and dehydrated in progressive EtOH solutions (25, 50, 75, 3× 100%). Samples were CO_2 critical point dried (Autosamdri-815, Tousimis, Rockville, MD) and palladium gold sputtered (DeskV, Denton Vacuum, Moores-town, NJ). Images were collected using a Hitachi S-4000 FE-SEM at 10 kV at 300× and 6000× magnification.

Contact angle measurements

Surface energy was evaluated using contact angle measurements and the Fowkes method. The contact angle of 25 μL drops of distilled water and ethylene glycol (Fisher Scientific, Pittsburg, PA) with the disc surface were determined by taking images with a Nikon D200 (Melville, NY) and determining contact angles with ImageJ software (NIH, Bethesda, MD). Using the Fowkes equation the interaction between the liquid and solid surface can be described as the following; $\gamma_L \left(1 + cos\, \theta\right) = 2\left(\sqrt{\gamma_L^d \gamma_S^d} + \sqrt{\gamma_L^p \gamma_S^p}\right)$. With θ being the angle formed by the droplet and the surface, and known polar (γ^p) and nonpolar dispersive (γ^d) adhesion parameters for water and ethylene glycol given by (γ_L = 72.8 mJ/m^2, γ_L^d = 21.8 mJ/m^2, γ_L^p = 51.0 mJ/m^2), and (γ_L = 78.0 mJ/m^2, γ_L^d = 29.0 mJ/m^2, γ_L^p = 19.0 mJ/m^2). Thus adhesion parameters of the solid, γ_S^d and γ_S^p, describe the overall surface energy of the solid tissue and can be found via a system of equations with the contact angles of the two liquids.[34,35]

Cell culture

Human umbilical cord Wharton's Jelly matrix cells (hWJMC) were used in all experiments. These stem cells have been shown to be an promising cell source for numerous tissue engineering applications, including TMJ regeneration.[36] Human umbilical cords were obtained from Labor & Delivery at Shands Hospital at the University of Florida (Gainesville, FL, IRB approval #64–2010) and cells were isolated via explant culture of the Wharton's Jelly matrix and used at passage 3. Lyophilized and sterilized discs were

rehydrated in DMEM supplemented with 10% FBS/1% Penicillin–Streptomycin (Thermo Scientific, Pittsburg, PA) in 96 well plates overnight before cell seeding. hWJMC were seeded onto the superior surface of the disc at a concentration of 2×10^3 cells/mm^3 and incubated at 37°C in 5% CO_2 humidified air.

After 24 h, constructs ($n = 6$) were assessed for initial cell adhesion. Constructs not collected for day 1 analysis were transferred to new wells with fresh media and incubated for an additional three days to evaluate sustained adhesion, proliferation, and viability ($n = 6$). At the time of collection, discs were gently rinsed in PBS and digested for 2 h at 37°C in 200 U/mL sterile filtered collagenase Type 1 (Life Technologies, Grand Island, NY). Following two freeze thaw cycles to lyse cells and release DNA, DNA quantification of the digest was performed using the Quant-IT Pico-green dsDNA assay (Life Technologies, Grand Island, NY) following manufacturer's instructions. Cell number was determined using the conversion of 7.7 pg DNA/cell.[37]

On day 4, viability and cell spreading ($n = 6$) was assessed with LIVE/DEAD fluorescent staining (Life Technologies, Grand Island, NY) on a Ziess Axio A1 inverted microscope (Zeiss, Gottingen, Germany). Three representative images per sample were acquired using an Axiocam ICc.1 at 20× objective magnification. Cell viability was quantified using ImageJ (NIH, Bethesda, MD) to count the quantity of dead and live cells. Furthermore, images were analyzed for the area of cell coverage using the thresholding technique. Cell migration and integration into the tissue was evaluated via histology. Tissues were embedded in Neg50 media (Richard Allen Scientific) and 10 μm sections were obtained with a HM 550 cryostat (Thermo Scientific). Sections were then stained with standard hematoxylin and eosin and mounted for evaluation.

Statistics

Statistical analysis was performed using SPSS software (Chicago, IL). One way ANOVA with a *post hoc* Tukey HSD test was used to determine significance ($\alpha = 0.05$). Mean and standard deviation were determined for all samples.

RESULTS

At 10% compressive strain representing physiologic strain values, the compressive modulus of the decellularized tissue scaffolds was not significantly affected by sterilization method when compared to the decellularized controls [Figure 2(A)]. However, at 20% strain used to determine bulk mechanical properties, all sterilization methods resulted in a significant ($p = 0.007, 0.007, 0.014$, respectively) decrease of ~80% instantaneous moduli from 500 kPa to 100–150 kPa. The steady state compressive modulus was unaffected with the exception of PAA treatments, which saw a decrease to 60 kPa as compared to 120 kPa for control tissue [$p = 0.014$, Figure 2(B)].

No appreciable differences in surface chemistry for Raman active vibrational modes were demonstrated between treatment methods (Figure 3). As expected, the spectra closely resemble that of pure collagen, which is the bulk constituent of the TMJ disc scaffolds.[38,39] FTIR spectra revealed several variations in surface chemistry of PAA and EtO sterilized

tissue as compared to the nonsterilized control (Figure 4). PAA and EtO discs presented broad peaks at 3600 cm^{-1} indicating the presence of additional hydroxyl groups (—OH). The original peak at 3350 cm^{-1} (maintained in GI treatments) correlates more closely with amine groups found in protein (—NH). PAA sterilized tissue showed further signs of oxidation by a lack of peak at 2900 cm^{-1} correlating with alkanes (C—H) and an additional peak at 1745 cm^{-1} attributed to carbonyl groups (C=O). Major peak assignments relevant to this analysis are shown in Table I.

SEM micrographs showed differences in ECM structural morphology resulting from exposure to each sterilization method (Figure 5). Treatments with PAA preserved fine collagen fiber definition and organization evidenced by its similarity to the decellularized control tissue. By contrast GI and EtO treatments showed damage of the collagen fiber matrix demonstrated by lack of fiber definition on the superior surface of the tissue and overall organizational disorder, which was much more pronounced in GI tissue than EtO treated tissue.

Wettability and the related surface free energy of the lyophilized tissues were determined by contact angle measurements. Hydration with deionized water (dH$_2$O) demonstrated that all tissue was hydrophilic defined by a contact angle <90°[Figure 6(A)]. PAA sterilized discs with contact angles averaging 40°were significantly more hydrophilic than controls that averaged 65°($p = 0.004$) and gamma-irradiated discs at 74°($p < 0.001$). EtO sterilized discs were more hydrophilic than the irradiated discs (contact angle = 52°, $p = 0.018$), but there was no statistical significance relative to controls ($p = 0.206$). Contact angle with dH$_2$O was not affected by the GI treatment. No significant differences were found between the surface free energy of the discs, but general trends indicated an increase in surface free energy for PAA and EtO sterilized discs [Figure 6(B)].

Initial adhesion and subsequent retention of hWJMC after 1 and 4 days showed superior cellular interactions of PAA sterilized scaffolds as compared to GI and EtO treatments (Figure 7). Approximately 90% of seeded cells adhered to PAA sterilized scaffolds (at 24 h postseeding) with a density of 1.7×10^3 cells/mm^3. This was more than three times the cell adhesion to GI and EtO treated scaffolds (0.48×10^3 cells/mm^3 and 0.22×10^3 cells/mm^3), respectively. After four days culture, cells continued to proliferate on PAA treated constructs demonstrated by a doubling in cell density while a reduction in density was noted on GI and EtO sterilized scaffolds.

LIVE/DEAD fluorescent staining was used to assess viable cell populations adhered to treated constructs. PAA and GI sterilized constructs showed adherent viable cells after four days culture (Figure 8, top row). A quantifiable high cell surface density was confirmed on PAA sterilized scaffolds as compared to the irradiated scaffold and EtO sterilized scaffolds [Figure 8(B)]. Qualitatively during image capture, cells were found adhered to not only the seeded superior surface of the PAA treated disc but on the inferior surface and sides. This is in contrast to irradiated scaffolds in which cells were localized only on the superior seeded surface and noticeably present on only three out of the six constructs evaluated. Cells on the EtO treated scaffolds generally displayed a more rounded morphology with some nonviable cells evident (Figure 8, top row). Quantification of cell viability showed an average of 80%

viability in EtO treated scaffolds compared to over 97% on GI and PAA treated scaffolds (Figure 8C).

Histological evaluation indicated no substantial cell infiltration had occurred over the four day culture period irrespective of sterilization method (Figure 9).

DISCUSSION

Different sterilization methods resulted in variations of the *ex vivo* derived fibrocartilage scaffold ultrastructure, mechanics, and chemistry that affected initial cell adhesion and continued cellular interactions *in vitro*. These changes modulated the biological responses and as such are a consideration for many biologically derived materials used for direct (or indirect) implantation.

SEM micrographs showed extensive alterations of the tissue microstructure when gamma irradiated and exposed to EtO. These effects are largely due to altered chemistry that weakens collagen fibrils. In a study of collagen fibril ultrastructure, Bailey et al.[22] showed loss of fibril definition in response to ionizing radiation. This was attributed to the rupture of hydrogen bonds and extensive protein scission induced by exposure to irradiation. Similarly, the reaction of EtO with the amine groups present in collagen molecules results in decreasing triple helix stability.[25] This decrease in stability may be responsible for similar structural alteration seen with GI treated tissues. Cell adhesion to protein in the ECM is mediated in part by integrins, which recognize specific peptide sequences. Many adhesion proteins in the ECM, including collagen, contain the arginine-glycine-aspartic acid (RGD) tripeptide.[40–42] The structural alterations induced by EtO and GI likely affected RGD and other cell binding sites within the collagen molecules contributing to inferior cell adhesion seen with both these treatments.

All sterilization methods affected material biomechanics including a significant reduction in the materials compressive instantaneous moduli when subjected to 20% compressive strain. For GI and EtO treated tissue, the weakening of normal collagen fibril structure associated with exposure may be responsible for this observation. The dose dependent effect of GI on graft biomechanical properties across a variety of tissues has been extensively documented.[4,22,43–45] When compared to the 10–35 kGy doses used in tissue banking, the results presented herein used a relatively low dose (13 kGy), yet still support other findings in that physical changes were clearly observed in SEM micrographs and further detected as biomechanical variation. PAA treated tissue also showed a decrease in compressive steady state moduli as compared to control values, whereas both EtO and GI displayed no significant variation. Some studies have shown PAA to increase porosity in collagenous tissue because of generation of oxygen within the tissue structure.[46,47] While PAA treatments have been shown to preserve many natural GAGs and proteins within tissue scaffolds, sterilization with PAA likely continued to elute additional soluble ECM protein during the sterilization as compared to the dry sterilization methods (EtO and GI).[12] These combined effects may account for the reduction in the materials steady state modulus.

Raman spectroscopy is commonly used to determine surface chemistry properties of soft tissue, as samples can be hydrated without interfering with the spectra. All Raman spectra were dominated by the collagen spectra showing strong amide 1, amide 2, and amide 3 peaks where expected and C—C stretch modalities associated with amino acids proline and hydroxyproline.[38,39] This suggests that following the decellularization protocol, the fibrocartilage scaffold was predominantly composed of Type 1 collagen, therefore these outcomes are relevant to collagen containing biomaterials.

FTIR is able to detect more polar bonds and functional groups and revealed excess hydroxylation (—OH) of EtO and PAA sterilized tissue. While generally attributed to water, all samples were equally desiccated prior to analysis. This peak could be linked to the byproducts of EtO previously mentioned, such as ethylene glycol (OH—CH_2CH_2—OH). More importantly, it is hypothesized that the additional hydroxyl groups in EtO sterilized discs are likely due to an alkylation reaction of the EtO molecule with the amino groups of the collagen polypeptide chains. Therefore, especially susceptible amino acids are arginine and lysine residues.[25,45] If EtO alkylates arginine residues, loss of RGD sites would occur, lowering cell adhesion potential.

PAA oxidizes aliphatic amino acid side chains, producing a mixture of ketones, aldehydes, and carboxylic acids, a mechanism which would contribute to the altered surface chemistry observed in PAA sterilized discs.[27] The occurrence of this mechanism is strongly supported by the absence of a defined peak at 2900 cm^{-1}, which correlates with alkanes (C—H), a peak that was displayed by all other tissue samples. The additional peaks at 3600 and 1745 cm^{-1} are attributed to the hydroxyl (—OH) and carbonyl groups (C=O), respectively, present in the oxidized compounds aforementioned. This reaction mechanism would not alter RGD sequences within the ECM, further supporting the maintenance of intrinsic cell adhesion following PAA sterilization.

Both PAA and EtO sterilized discs showed a decrease in dH_2O contact angle and trended toward an increased surface free energy, which can be attributed to the surface chemistry changes, namely an increase of polar surface functional groups as determined by FTIR analysis. By comparison, as GI produced no detectable changes in surface chemistry, it is not surprising that contact angle and surface free energy of the GI discs was identical to control discs. Hydrophilicity and wettability are closely related and in synthetic biomaterials an important parameter for adhesion of proteins and cells. Adsorption of serum protein to biomaterial surfaces may precede and facilitate adhesion of cells to implanted materials. However, variable results have been reported regarding whether hydrophilic or hydrophobic surfaces better promote protein adsorption, likely because of the diversity of protein structure and charged surface groups.[48,49] There have been many controlled studies on synthetic materials in which have examined cell adhesion in relation to wettability. It has been found that cells and adhesive proteins adhere to wettable surfaces with contact angles ranging from 40 to 70.[50–52] However other factors, such as surface functional groups, also play an important role in cell adhesion.[53,54]

The importance of hydroxyl groups to facilitate cell adhesion to a variety of surfaces has been previously recognized.[48,55,56] Investigations by Keselowsky et al. looked specifically

at cell focal adhesion molecules as a function of controllable surface chemistry. It was found that the highest rates of adhesion were linked to hydroxyl (OH) groups followed by carboxylic acid (COOH) and amine (NH$_2$) groups.[56] This work directly supports the increased adhesion seen in the PAA sterilized scaffolds and mirrors the surface chemistry changes observed as compared to control tissue.

As a final observation, viable cells were visualized on all surfaces of the PAA treated constructs. The substantially higher initial adhesion of cells contributed to the increased cell densities observed on day 4. While cells adhered to GI constructs were viable, cell adhesion was low after four days and the result of inferior cell interactions during culture. This was contrasted by the low cell density and viability observed and quantified on EtO sterilized constructs. This was likely due to byproducts of EtO sterilization that were retained after extensive aeration time, demonstrating that EtO sterilization of thick tissue has significant drawbacks. These results emulate the clinical observation that byproducts from EtO treated grafts are released after implantation leading to pathological reactions.[17] This also accounts for lower cell numbers in EtO treated constructs as compared to the PAA treatments, even though EtO scaffolds showed adhesion promoting surface chemistry similar to PAA treated scaffolds.

CONCLUSION

By their very nature, terminal sterilization techniques are designed to result in effective sterilization. These aggressive processes also initiate a variety of structural, biomechanical, and chemical changes often detrimental to the biomaterial tissue matrix. While other biological tissues have the potential to respond differently to the sterilants evaluated in this study, exposure of tissue to GI and EtO resulted in extensive damage to the scaffolds microstructure. In addition, all sterilization techniques assessed in these investigations weakened compressive biomechanical properties of the fibrocartilage scaffolds. Relative to GI and EtO, PAA sterilization limited physical change, while inducing chemical modifications that favored cell attachment, including hydroxylation and increased surface hydrophilicity. Studying cell attachment to ECM-based scaffolds *in vitro* provides further insight into the use of these methods for sterilizing soft tissue grafts before clinical translation, evidenced by cell interaction with EtO treated constructs and clinical outcomes observed using EtO sterilized grafts.

ACKNOWLEDGMENTS

REFERENCES

1. Deumens R, Bozkurt A, Meek MF, Marcus MA, Joosten EA, Weis J, Brook GA. Repairing injured peripheral nerves: Bridging the gap. Prog Neurobiol. 2010; 92:245–276. [PubMed: 20950667]

2. Bauer TW, Muschler GF. Bone graft materials. An overview of the basic science. Clin Orthop Relat Res. 2000:10–27. [PubMed: 10693546]

3. Lindford AJ, Kaartinen IS, Virolainen S, Kuokkanen HO, Vuola J. The dermis graft: Another autologous option for acute burn wound coverage. Burns. 2012; 38:274–282. [PubMed: 21903331]

4. Vangsness CT Jr, Garcia IA, Mills CR, Kainer MA, Roberts MR, Moore TM. Allograft transplantation in the knee: Tissue regulation, procurement, processing, and sterilization. Am J Sports Med. 2003; 31:474–481. [PubMed: 12750147]

5. Moore M, Moore R, McFetridge PS. Directed oxygen gradients initiate a robust early remodeling response in engineered vascular grafts. Tissue Eng Part A. 2013; 19:2005–2013. [PubMed: 23541106]

6. Lumpkins SB, Pierre N, McFetridge PS. A mechanical evaluation of three decellularization methods in the design of a xenogeneic scaffold for tissue engineering the temporomandibular joint disc. Acta Biomater Engl. 2008; 4:808–816.

7. Schmidt CE, Baier JM. Acellular vascular tissues: natural biomaterials for tissue repair and tissue engineering. Biomaterials. 2000; 21:2215–2231. [PubMed: 11026628]

8. Badylak SF. Xenogeneic extracellular matrix as a scaffold for tissue reconstruction. Transpl Immunol. 2004; 12:367–377. [PubMed: 15157928]

9. Crapo PM, Gilbert TW, Badylak SF. An overview of tissue and whole organ decellularization processes. Biomaterials. 2011; 32:3233–3243. [PubMed: 21296410]

10. Uzarski JS, Van De Walle AB, McFetridge PS. Preimplantation processing of ex vivo-derived vascular biomaterials: effects on peripheral cell adhesion. J Biomed Mater Res A. 2013; 101:123–131. [PubMed: 22825780]

11. Goktas S, Matuska AM, Pierre N, Gibson TM, Dmytryk JJ, McFetridge PS. Decellularization method influences early remodeling of an allogenic tissue scaffold. J Biomed Mater Res A. 2014; 102A:8–16. [PubMed: 23468315]

12. Gilbert TW, Sellaro TL, Badylak SF. Decellularization of tissues and organs. Biomaterials. 2006; 27:3675–3683. [PubMed: 16519932]

13. Amensag S, McFetridge PS. Rolling the human amnion to engineer laminated vascular tissues. Tissue Eng Part C Methods. 2012; 18:903–912. [PubMed: 22616610]

14. Dziedzic-Goclawska A, Kaminski A, Uhrynowska-Tyszkiewicz I, Stachowicz W. Irradiation as a safety procedure in tissue banking. Cell Tissue Bank. 2005; 6:201–219. [PubMed: 16151960]

15. Nguyen H, Morgan DA, Forwood MR. Sterilization of allograft bone: Effects of gamma irradiation on allograft biology and bio-mechanics. Cell Tissue Bank. 2007; 8:93–105. [PubMed: 17063262]

16. Mendes GC, Brandao TR, Silva CL. Ethylene oxide sterilization of medical devices: A review. Am J Infect Control. 2007; 35:574–581. [PubMed: 17980234]

17. Huang Q, Dawson RA, Pegg DE, Kearney JN, Macneil S. Use of peracetic acid to sterilize human donor skin for production of acellular dermal matrices for clinical use. Wound Repair Regen. 2004; 12:276–287. [PubMed: 15225206]

18. Holy CE, Cheng C, Davies JE, Shoichet MS. Optimizing the sterilization of PLGA scaffolds for use in tissue engineering. Biomaterials. 2001; 22:25–31. [PubMed: 11085380]

19. Hirota N, Mizuno K, Goto Y. Group additive contributions to the alcohol-induced alpha-helix formation of melittin: implication for the mechanism of the alcohol effects on proteins. J Mol Biol. 1998; 275:365–378. [PubMed: 9466915]

20. Conway K, Kiernan JA. Chemical dehydration of specimens with 2,2-dimethoxypropane (DMP) for paraffin processing of animal tissues: Practical and economic advantages over dehydration in ethanol. Biotech Histochem. 1999; 74:20–26. [PubMed: 10190257]

21. Grabenwoger M, Sider J, Fitzal F, Zelenka C, Windberger U, Grimm M, Moritz A, Bock P, Wolner E. Impact of glutaraldehyde on calcification of pericardial bioprosthetic heart valve material. Ann Thorac Surg. 1996; 62:772–777. [PubMed: 8784007]

22. Bailey AJ, Tromans WJ. Effects of ionizing radiation on the ultra-structure of collagen fibrils. Radiat Res. 1964; 23:145–155. [PubMed: 14218078]

23. Salehpour A, Butler DL, Proch FS, Schwartz HE, Feder SM, Doxey CM, Ratcliffe A. Dose-dependent response of gamma irradiation on mechanical properties and related biochemical

composition of goat bone-patellar tendon-bone allografts. J Orthop Res. 1995; 13:898–906. [PubMed: 8544027]

24. Cheung DT, Perelman N, Tong D, Nimni ME. The effect of gamma-irradiation on collagen molecules, isolated alpha-chains, and cross-linked native fibers. J Biomed Mater Res. 1990; 24:581–589. [PubMed: 2324128]

25. Olde Damink LH, Dijkstra PJ, Van Luyn MJ, Van Wachem PB, Nieuwenhuis P, Feijen J. Influence of ethylene oxide gas treatment on the in vitro degradation behavior of dermal sheep collagen. J Biomed Mater Res. 1995; 29:149–155. [PubMed: 7738061]

26. Chassot AL, Poisl MI, Samuel SM. In vivo and in vitro evaluation of the efficacy of a peracetic acid-based disinfectant for decontamination of acrylic resins. Braz Dent J. Brazil. 2006; 17:117–121.

27. Finnegan M, Linley E, Denyer SP, McDonnell G, Simons C, Maillard JY. Mode of action of hydrogen peroxide and other oxidizing agents: Differences between liquid and gas forms. J Anti-microb Chemother. 2010; 65:2108–2115.

28. Haimi S, Vienonen A, Hirn M, Pelto M, Virtanen V, Suuronen R. The effect of chemical cleansing procedures combined with peracetic acid-ethanol sterilization on biomechanical properties of cortical bone. Biologicals. 2008; 36:99–104. [PubMed: 17892947]

29. Johns DE, Athanasiou KA. Design characteristics for temporomandibular joint disc tissue engineering: Learning from tendon and articular cartilage. Proc Inst Mech Eng H. 2007; 221:509–526. [PubMed: 17822153]

30. Scheffler SU, Scherler J, Pruss A, von Versen R, Weiler A. Biomechanical comparison of human bone-patellar tendon-bone grafts after sterilization with peracetic acid ethanol. Cell Tissue Bank. 2005; 6:109–115. [PubMed: 15909098]

31. Kim KW, Wong ME, Helfrick JF, Thomas JB, Athanasiou KA. Bio-mechanical tissue characterization of the superior joint space of the porcine temporomandibular joint. Ann Biomed Eng. 2003; 31:924–930. [PubMed: 12918907]

32. Juran CM, Dolwick MF, McFetridge PS. Shear mechanics of the TMJ disc: Relationship to common clinical observations. J Dent Res. 2013; 92:193–198. [PubMed: 23166043]

33. Ali SM, Bonnier F, Lambkin H, Flynn K, McDonagh V, Healy C, Lee TC, Lyng FM, Byrne HJ. A comparison of Raman, FTIR and ATR-FTIR micro spectroscopy for imaging human skin tissue sections. Anal Methods. 2013; 5:2281–2291.

34. Fowkes FM. Attractive forces at interfaces. Indus Eng Chem. 1964; 56:40–52.

35. Cwikel D, Zhao Q, Liu C, Su X, Marmur A. Comparing contact angle measurements and surface tension assessments of solid surfaces. Langmuir. 2010; 26:15289–15294. [PubMed: 20815356]

36. Bailey MM, Wang L, Bode CJ, Mitchell KE, Detamore MS. A comparison of human umbilical cord matrix stem cells and temporomandibular joint condylar chondrocytes for tissue engineering temporomandibular joint condylar cartilage. Tissue Eng. 2007; 13:2003–2010. [PubMed: 17518722]

37. Hoemann CD, Sun J, McKee MD, Chevrier A, Rossomacha E, Rivard GE, Hurtig M, Buschmann MD. Chitosan-glycerol phosphate/blood implants elicit hyaline cartilage repair integrated with porous subchondral bone in microdrilled rabbit defects. Osteoarthr Cartil. 2007; 15:78–89. [PubMed: 16895758]

38. Wang YN, Galiotis C, Bader DL. Determination of molecular changes in soft tissues under strain using laser Raman microscopy. J Biomech. 2000; 33:483–486. [PubMed: 10768397]

39. Ogawa M, Harada Y, Yamaoka Y, Fujita K, Yaku H, Takamatsu T. Label-free biochemical imaging of heart tissue with high-speed spontaneous Raman microscopy. Biochem Biophys Res Commun. 2009; 382:370–374. [PubMed: 19285035]

40. Widgerow AD. Bioengineered matrices. Part 2: Focal adhesion, integrins, and the fibroblast effect. Ann Plast Surg. 2012; 68:574–578. [PubMed: 22643102]

41. Ruoslahti E, Pierschbacher MD. New perspectives in cell adhesion: RGD and integrins. Science. 1987; 238:491–497. [PubMed: 2821619]

42. Hersel U, Dahmen C, Kessler H. RGD modified polymers: Biomaterials for stimulated cell adhesion and beyond. Biomaterials. 2003; 24:4385–4415. [PubMed: 12922151]

43. Balsly CR, Cotter AT, Williams LA, Gaskins BD, Moore MA, Wolfinbarger L. Effect of low dose and moderate dose gamma irradiation on the mechanical properties of bone and soft tissue allografts. Cell Tissue Bank. 2008; 9:289–298. [PubMed: 18431690]

44. Fideler BM, Vangsness CT, Lu B, Orlando C, Moore T. Gamma irradiation: Effects on biomechanical properties of human bone-patellar tendon-bone allografts. Am J Sports Med. 1995; 23:643–646. [PubMed: 8526284]

45. Friess W. Collagen—Biomaterial for drug delivery. Eur J Pharm Biopharm. 1998; 45:113–136. [PubMed: 9704909]

46. Lomas RJ, Jennings LM, Fisher J, Kearney JN. Effects of a peracetic acid disinfection protocol on the biocompatibility and bio-mechanical properties of human patellar tendon allografts. Cell Tissue Bank. 2004; 5:149–160. [PubMed: 15509904]

47. Woon CY, Pridgen BC, Kraus A, Bari S, Pham H, Chang J. Optimization of human tendon tissue engineering: peracetic acid oxidation for enhanced reseeding of acellularized intrasynovial tendon. Plast Reconstr Surg. 2011; 127:1107–1117. [PubMed: 21364414]

48. Gao J, Niklason L, Langer R. Surface hydrolysis of poly(glycolic acid) meshes increases the seeding density of vascular smooth muscle cells. J Biomed Mater Res. 1998; 42:417–424. [PubMed: 9788505]

49. Xu LC, Siedlecki CA. Effects of surface wettability and contact time on protein adhesion to biomaterial surfaces. Biomaterials. 2007; 28:3273–3283. [PubMed: 17466368]

50. Borges AM, Benetoli LO, Licinio MA, Zoldan VC, Santos-Silva MC, Assreuy J, Pasa AA, Debacher NA, Soldi V. Polymer films with surfaces unmodified and modified by non-thermal plasma as new substrates for cell adhesion. Mater Sci Eng C Mater Biol Appl. 2013; 33:1315–1324. [PubMed: 23827577]

51. Grinnell F. Cellular adhesiveness and extracellular substrata. Int Rev Cytol. 1978; 53:65–144. [PubMed: 208994]

52. Barrias CC, Martins MC, Almeida-Porada G, Barbosa MA, Granja PL. The correlation between the adsorption of adhesive proteins and cell behaviour on hydroxyl-methyl mixed self-assembled monolayers. Biomaterials. 2009; 30:307–316. [PubMed: 18952279]

53. Arima Y, Iwata H. Effect of wettability and surface functional groups on protein adsorption and cell adhesion using well-defined mixed self-assembled monolayers. Biomaterials. 2007; 28:3074–3082. [PubMed: 17428532]

54. Lee JH, Lee JW, Khang G, Lee HB. Interaction of cells on chargeable functional group gradient surfaces. Biomaterials. 1997; 18:351–358. [PubMed: 9068898]

55. Curtis AS, Forrester JV, McInnes C, Lawrie F. Adhesion of cells to polystyrene surfaces. J Cell Biol. 1983; 97:1500–1506. [PubMed: 6355120]

56. Keselowsky BG, Collard DM, Garc ıa AJ. Surface chemistry modulates focal adhesion composition and signaling through changes in integrin binding. Biomaterials. 2004; 25:5947–5954. [PubMed: 15183609]
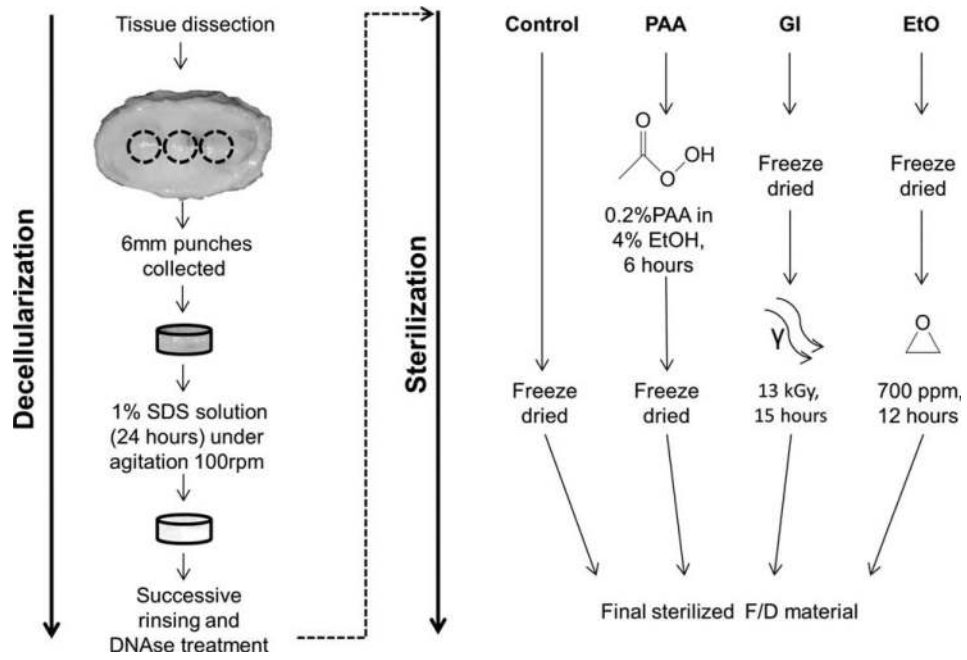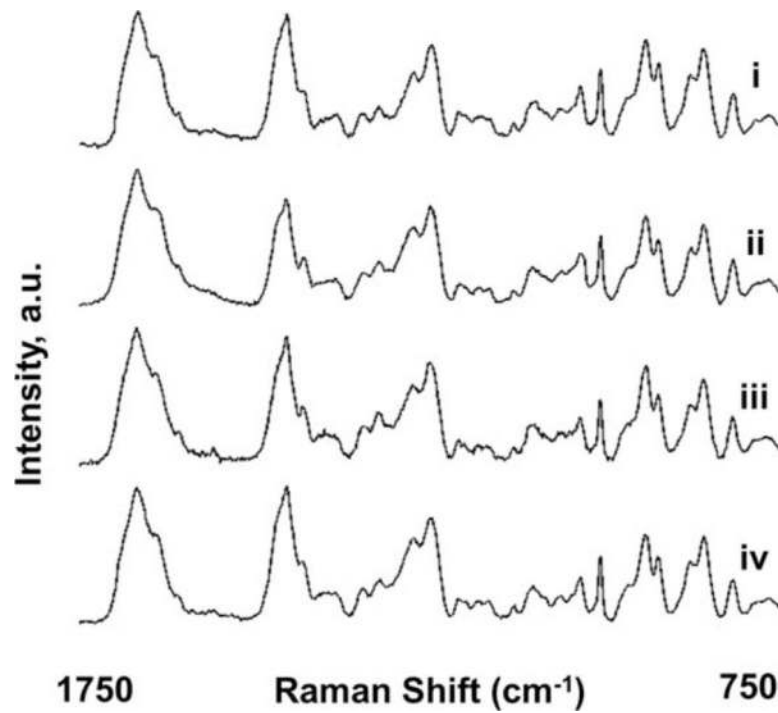
FIGURE 1.

Schematic of decellularization and sterilization. Diagram outlining pTMJ decellularization with 1% SDS and subsequent sterilization with PAA, GI, and EtO.
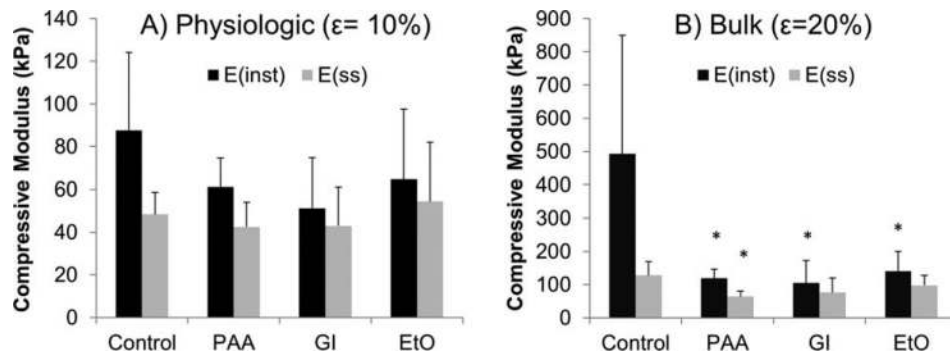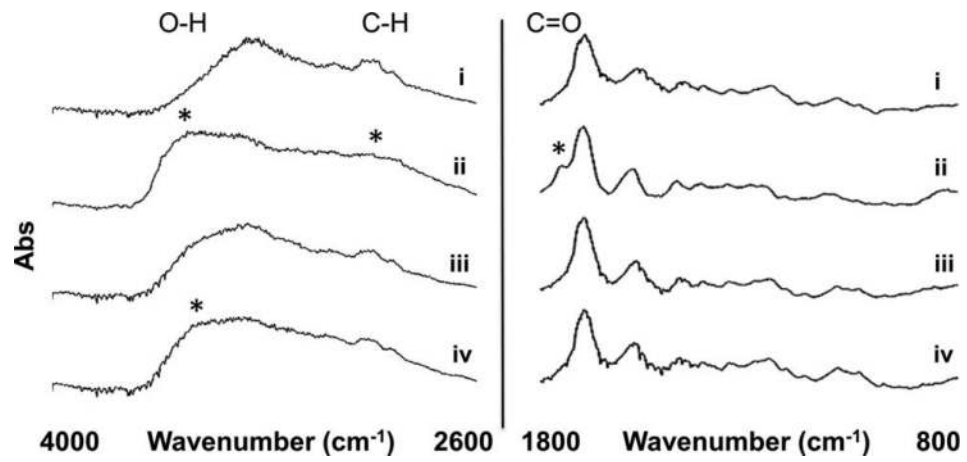
FIGURE 2.

Effect of sterilization on physiologic and bulk mechanical properties. (A) Physiologic and (B) bulk material instantaneous (inst) and steady state (ss) compressive moduli. Physiologic strain (10%) and super physiologic strain (20%) were used (*) indicates statistical significance compared to controls ($n = 6$, $\alpha = 0.05$).

FIGURE 3.
Comparison of surface chemistry by Raman spectroscopy. The (i) control, (ii) PAA, (iii) GI, and (iv) EtO sterilized scaffold Raman spectra ($n = 9$) from 1750 to 750 cm^{-1}. No distinct variation existed between the control and sterilized discs.
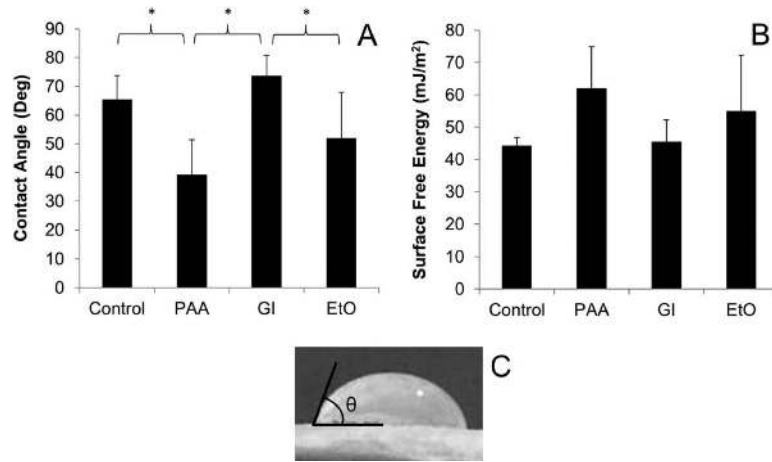
FIGURE 4.
Comparison of surface chemistry by FTIR spectroscopy. The (i) control, (ii) PAA, (iii) GI, and (iv) EtO sterilized disc FTIR spectra ($n = 9$) from 4000 to 2600 cm^{-1} and 1800–800 cm^{-1}. Variations in spectra from control discs are denoted with a (*).
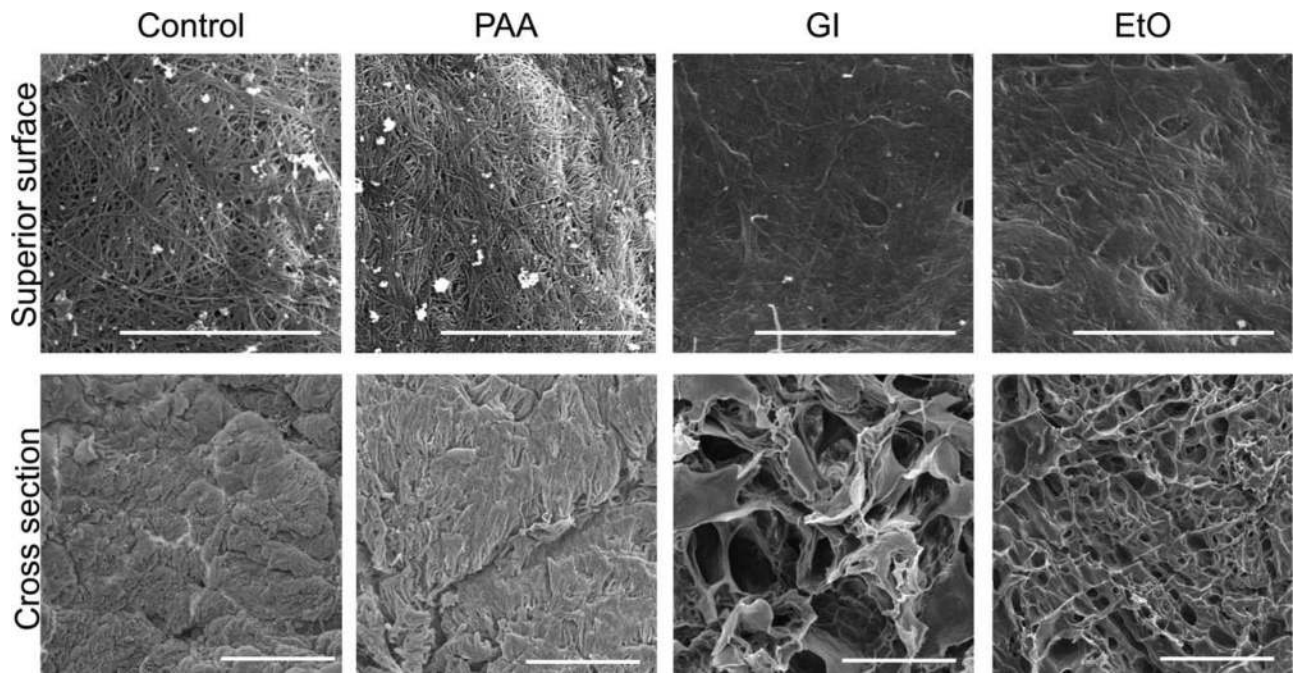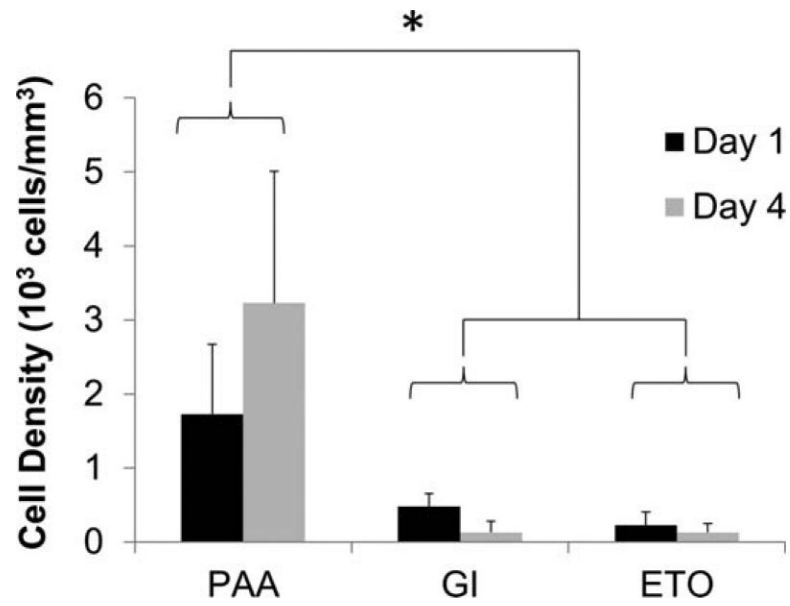
FIGURE 5.

Microstructural analysis of tissue. SEM images taken of the superior surface at 6000× (top row) and the cut cross-section at 300× (bottom row) magnification demonstrating physical modifications of the tissue as a result of sterilization method. Different magnification was chosen to show appropriate detail level for each surface. Scale bars represents 5 and 100 μm, respectively.
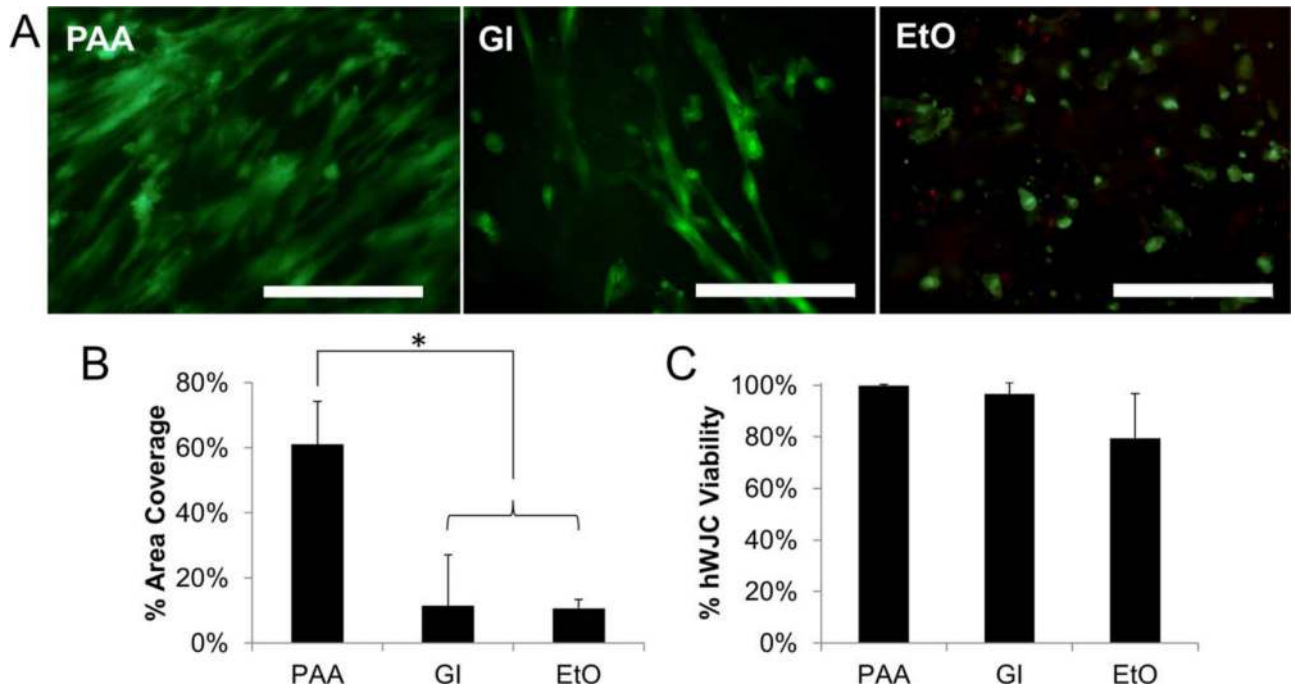
FIGURE 6.
Wettability and surface free energy of the scaffolds. (A) Average contact angle with dH$_2$O and (B) calculated surface free energy of the scaffolds ($n = 6$). All surfaces were considered hydrophilic (<90°). (C) A sample contact angle measurement. (*) indicates statistically significant difference between sterilization method ($\alpha = 0.05$).
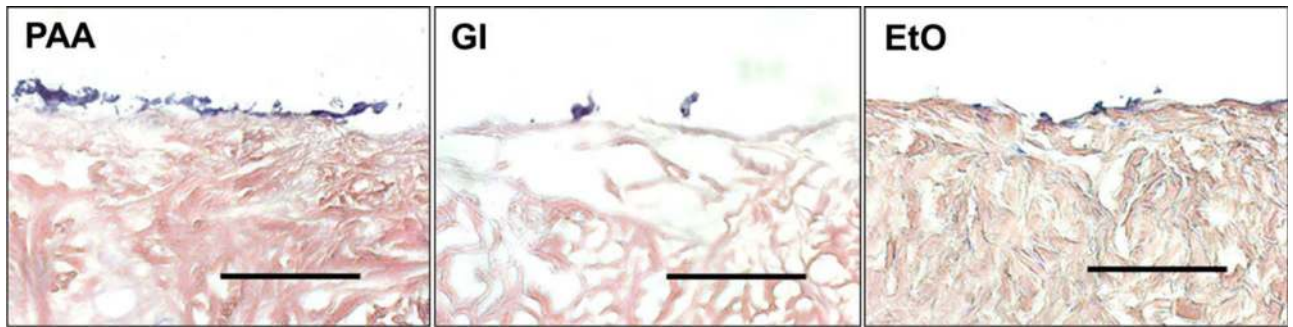
FIGURE 7.

Initial cell adhesion and proliferation. Cell number per volume of disc scaffold after 1 and 4 days of static culture. (*) indicates statistically significant difference between sterilization method for both time points (α = 0.05).

FIGURE 8.

Cellular viability and cell coverage. (A) Calcien AM/ethidium homodimer staining demonstrated difference in cell viability and morphology on differentially sterilized scaffolds after 4 days (top row, living cells stain green while dead cells stain red). Scale bars indicate 200 μm. B) Average percent of the scaffold area covered by cells in images. C) Average cell viability determined from images. (*) indicates statistically significant difference between sterilization methods (α = 0.05). [Color figure can be viewed in the online issue, which is available at wileyonlinelibrary.com.]

FIGURE 9.

Cell migration. Histology indicated no noticeable migration into tissue after the four day culture period for any of the scaffold sterilization methods. Scale bars indicate 200 μm. [Color figure can be viewed in the online issue, which is available at wileyonlinelibrary.com.]

TABLE I

Raman and IR Frequencies Relevant to Peak Assignments, With Intensity Described for Each As Either Weak (W), Medium (M), or Strong (S)

Assignment	Vibration mode	Frequency Range (cm^{-1})	Raman	FTIR
Hydroxyl	O–H stretch	3600-3200	W	S
Amide 1	N–H stretch	3500-3300		M
Alkane	C–H stretch	2950-2850		S
Carbonyl/ester	C=O stretch	1750-1735	W	S
Amide 1	C=O stretch	1630-1690	M-S	S
Amide 2	N–H bend	1550-1560	W	S
Amide 3	C–N stretch, N–H bend	1230-1280	var	W-M
Hydroxyproline, proline	C–C stretch	856-875		